

Transition Flight Modeling of a Fixed-Wing VTOL UAV

B. Yuksek · A. Vuruskan · U. Ozdemir ·
M. A. Yukselen · G. Inalhan

Received: 15 December 2014 / Accepted: 28 December 2015 / Published online: 11 January 2016
© Springer Science+Business Media Dordrecht 2016

Abstract This paper describes a complete six-degree-of-freedom nonlinear mathematical model of a tilt rotor unmanned aerial vehicle (UAV). The model is specifically tailored for the design of a hover to forward flight and forward flight to hover transition control system. In that respect, the model includes the aerodynamic effect of propeller-induced airstream which is a function of cruise speed, tilt angle and angle of attack. The cross-section area and output velocity of the propeller-induced airstream are calculated with momentum theory. The projected area on the UAV body that is affected by the propeller-induced airstream is specified and 2D aerodynamic analyses are performed for the airfoil profile of this region. Lookup-tables are generated and implemented in the nonlinear mathematical model. In addition, aerodynamic coefficients of the airframe are calculated by using CFD method and these data are embedded

into the nonlinear model as a lookup-table form. In the transition flight regime, both aerodynamic and thrust forces act on the UAV body and the superimposed dynamics become very complex. Hence, it is important to define a method for hover-to-cruise and cruise-to-hover transitions. To this end, both transition scenarios are designed and a state-schedule is developed for flight velocity, angle of attack, and thrust levels of each of the thrust-propellers. This transition state schedule is used as a feedforward state for the flight control system. We present the simulation results of the transition control system and show the successful transition of TURAC in experiment.

Keywords Transition flight modeling · VTOL UAV · Tilt rotor · Simulation · Control

1 Introduction

In recent years, civil UAVs have been used widely in areas such as agricultural observation, wildlife protection, and traffic monitoring. There are various types of UAVs such as quadrotor, tilt-rotor/tilt-wing and vertical take-off and landing UAV, etc. which are each designed for different operational aims. Each of these airframe concepts has advantages and disadvantages depending on the design.

Unmanned rotorcrafts are able to take-off and land vertically on both flat and rugged surfaces. They do not need a helipad because of their low weight and small dimensions. Observation and reconnaissance

B. Yuksek (✉) · A. Vuruskan · U. Ozdemir ·
M. A. Yukselen · G. Inalhan
Faculty of Aeronautics and Astronautics, Istanbul Technical
University, 34469 Istanbul, Turkey
e-mail: yuksekb@itu.edu.tr

A. Vuruskan
e-mail: vuruskan@itu.edu.tr

U. Ozdemir
e-mail: ugur.ozdemir@itu.edu.tr

M. A. Yukselen
e-mail: yukselen@itu.edu.tr

G. Inalhan
e-mail: inalhan@itu.edu.tr

missions of a specified area can be performed for several minutes while hovering, which is the most important capability of the unmanned rotorcrafts.

Despite the advantages of the hover flight regime, unmanned rotorcrafts cannot be used for operations which require higher speeds, longer flight ranges or larger payload capacities. Compared to the rotorcrafts, fixed-wing UAVs have remarkable payload capacities for different types of operations such as logistics and high altitude observation.

Especially in military applications, it is important to be able to operate UAVs in variable conditions. Depending on the combat area, it may be necessary to land and take off from difficult terrain such as steep slopes and uneven surfaces. In addition, UAVs may operate in multiple flight regimes during a surveillance operation that requires tracking static and moving targets.

These requirements are relevant not only for military operations but also for civilian applications such as detecting cracks or leakages in pipelines, performing surveillance of a moving or static target in urban traffic, or transporting emergency medical supplies between medical storage facilities, hospitals, and clinics in both cities and the countryside. Runways may not be available in these areas. Especially in urban areas, it may be necessary to landing and takeoff in a limited area such as the roof of a building. If operation time is an important factor, aircraft design should combine the high-speed cruising capability of fixed-wing UAVs and the hovering and vertical take-off/landing capability of rotary-wing UAVs. For this reason, recent studies have focused on fixed-wing VTOL concepts that combine the advantages of fixed-wing and rotary-wing UAVs.

There are several VTOL UAV concepts with tilt-wing, tail-sitter, and tilt-rotor designs [1]. Tilt-wing UAVs take off and land vertically with a tilted-wing propulsion system. Initially, they start to climb vertically and altitude increases. During the transition flight regime, the tilt angle of the wing gradually decrease toward the horizontal position before the UAV starts to accelerate. After reaching stall speed, the wing-propulsion system is oriented horizontally and transition flight regime is completed. Tail-sitter UAVs do not have wing or propulsion system with tilt mechanisms but instead have pusher or tractor propellers. At the beginning of the flight, the UAV accelerates vertically to increase altitude. Then it performs

the transition from hover to horizontal flight, which is the most critical point. In practice, the transition is achieved by a crucial stall-and-tumble maneuver. For this reason, controlled transition scenarios and maneuvers are developed to minimize crash probability. In tilt-rotor models, the propulsion system can be positioned vertically or horizontally depending on the flight regime. Tilt-rotor UAVs behave like helicopters during hover flight and operations can be performed in this flight regime. As tilt angle decreases toward the horizontal position, the UAV starts to accelerate. After the UAV's velocity is about 1.2 times faster than the stall speed, the tilt-rotors are positioned horizontally and the transition flight regime is completed. During the transition flight, it is important to follow a transition schedule to reach the trim point. To accomplish this reliably, transition scenarios are developed that supply the required flight velocity and angle of attack data to the flight control system.

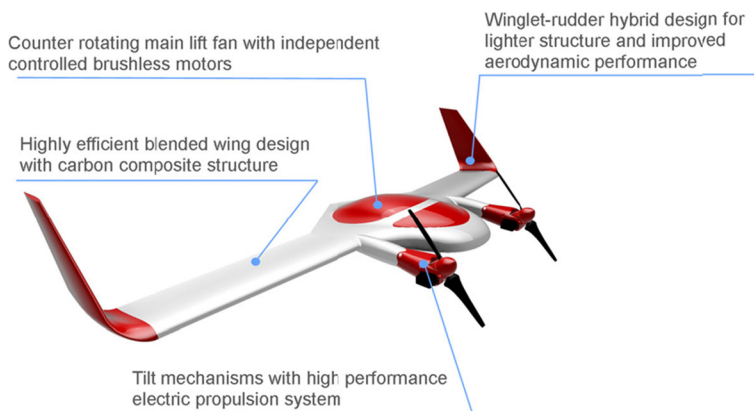
Driven by the below design requirements [2];

- 1 hr cruise flight + 10 min hover flight + 15 min takeoff and landing 70 km operation flight range
- 20 m/s cruise speed
- 8 kg payload
- Automatic takeoff/landing flight control system

and following the above-mentioned advantages associated with tilt-rotor VTOL UAVs, “TURAC” is designed and prototyped by the Control and Avionics Laboratory of the Istanbul Technical University [3]. General view of the TURAC is given in Fig. 1. It is important to note that, besides various academic researchers, several companies are also working on tilt-rotor UAV designs. Commercial fixed-wing tilt-rotor UAVs include the Panther (Israel Aerospace Industries), Eagle Eye (Bell Helicopter), AD-150 (American Dynamics Flight System), and Phantom Swift (Boeing), which were all developed for military applications. In that respect, TURAC is tailored towards civilian applications and the design embeds various distinct and novel concepts.

TURAC design has a blended-wing airframe that generates lift with both the body (in the closed coaxial fan configuration) and the wings. For longitudinal static stability, reflex airfoil profiles are used instead of a tail group. In this way, the lift force capacity is increased while the drag force remains at an acceptable level. The wings and winglets are detachable, an advantage for easy transportation and adjusting the

Fig. 1 General view of TURAC



wingspan according to mission requirements. The all-electrical propulsion system includes brushless direct-current motors and Lithium Polymer batteries that provide high performance.

TURAC has two tilt-rotors which are mounted on the port- and starboard-front of the body. Each tilt-rotor group provides the 15 % (and up to maximum 30 %) of the total weight of the UAV and they are active during the hover, transition and cruise flight regimes. A co-axial lifting fan group is mounted on the rear part of the body and it is embedded into the airframe. In hover and transition flight regimes, the co-axial fan group becomes active and provides the vertical thrust force about 70 % of the total UAV weight.

In hover flight regime, tilt-rotors are positioned upward and the co-axial fan group is activated. Then the UAV increases its altitude to a predefined safety level before the transition. In the transition flight regime, tilting mechanisms start to rotate toward the horizontal position to generate horizontal thrust force and this acceleration phase is kept until the forward flight speed reaches about 1.2 times of the stall speed. When the UAV exceeds the stall speed, the rotations

of the tilt rotors are completed and the UAV enters the horizontal flight regime.

For hover, forward flight and transition flight tests, several scaled prototypes of TURAC are manufactured by using rapid-prototyping techniques [3, 4]. Flight test are performed on various 1/2 - 1/3 scale models of TURAC due to the limited flight test area on the university campus. So, mathematical modeling studies are performed on this prototype to verify flight tests and simulations. 1/3 scale prototype is shown in Fig. 2 and a photo from hover test flight is shown Fig. 3. We refer the reader to [3, 4] for an extensive treatment of not only the design but also the prototype manufacturing process of TURAC.

Table 1 lists basic characteristics of the prototype. Inertia moments are calculated from bifilar (two wire) pendulum tests.

In this paper we focus on the dynamic modeling of the TURAC fixed-wing VTOL. Specifically, we introduce a complete six-degree-of-freedom nonlinear mathematical model which model is tailored for the design of a hover to forward flight and vice-versa transition control system. In the transition flight regime, both aerodynamic and thrust forces act on

Fig. 2 1/3 scale prototype of the TURAC



Fig. 3 1/3 scale TURAC in hover flight test



the UAV body and dynamics become very complex. Hence, it is important to define a transition corridor for hover-to-cruise and cruise-to-hover flight. To this end, both transition scenarios are described based on the balance of forces and moments on the UAV. A schedule is developed for flight velocity, angle of attack, and thrust levels of each propeller and is used as a feed-forward data set for the flight control system.

This paper is organized in the following way; In Section 2, we provide a review of the related theoretical works associated with VTOL UAV modeling and control. In Section 3, general nonlinear equations of motion with six degrees of freedom are derived for the complete flight regime from hover to horizontal flight. Aerodynamic effects of free airstream and propeller induced airstream are modeled separately by using aerodynamic data which are obtained from CFD analysis. These datasets are used to generate aerodynamic lookup-tables. Thrust – flight speed test results of the propeller that used in tilt-rotor assembly is obtained from the manufacturer's data base and an additional lookup-table is generated for this relationship.

Table 1 Specifications of the 1/3 Scale TURAC prototype

Wingspan	1.73 m
Length	0.6 m
Maximum takeoff weight	5.5 kg
I_{xx}	0.26198 kg.m^2
I_{yy}	0.05 kg.m^2
I_{zz}	0.5525 kg.m^2
$I_{xz}=I_{zx}$	$\approx 0 \text{ kg.m}^2$
Cruise speed	35 m/s

Transition scenarios are generated for hover-to-cruise and cruise-to-hover flight regimes based on mathematical expressions and CFD analysis. A reference signal schedule for transition control system is generated by using these scenario dataset. In Section 4, the general closed-loop control system is described. Transition and back-transition algorithms are explained step-by-step. Real-time hover-to-cruise and cruise-to-hover simulations are performed based on the transition scenario and results are given. In addition we show the successful transition of TURAC in experiment. Concluding remarks are made in Section 5.

2 Related Theoretical Works

Aerodynamic analysis of VTOL fixed wing air vehicles can be divided up as aerodynamic analyses of hover, transition, and forward flight regimes. For the hover regime, numerous studies have been done experimentally and numerically. In [5], a quad tilt-rotor in hover mode is modeled and analyzed by using the CFD method. The pressure distribution on the wing, flow-field around the vehicle, and spanwise loading is investigated in and out of ground effect. Another study [6], which includes CFD analyses of a full and half-span V-22 tilt-rotor configuration in hover mode, has been done in order to observe flow-field around the vehicle. Rotor performance differences between two different models are evaluated. In [7], rotor/wing interaction, aircraft aerodynamics, pressure distribution, and force loading along wingspan are experimentally investigated on a quarter-scale V-22 tilt-rotor aircraft in hover mode.

For forward flight regime, performance and design of conventional tilt-rotors and quad tilt-rotors have been investigated in [8]. Here, lift-to-drag ratio for both concepts is based on interference, reduction in rotor tip speed, and the change on rotor rotational direction. The UAVs are tested and analyzed using wind tunnels and CFD methods to define flowfield around the airframe and aerodynamic coefficients [9, 10]. Propeller/wing interaction on multi-engine transport aircraft is investigated by modeling the propeller as an actuator disk, as in the CFD method [11]. Furthermore, aerodynamic stability and control coefficients of TR-E2S1 tilt-rotor aircraft are calculated with the CFD method and the wind tunnel tests. The results from both methods are evaluated and compared at the end of the study [12]. The same methods are applied to V-22 Osprey tilt-rotor aircraft in forward flight regime [13]. In [14], Yak-54 is analyzed aerodynamically and results are compared from Vorstab, Fluent, and Aircraft Advanced Analysis (AAA). In these study, the area on the wing affected by propeller cannot be specify exactly by using CFD methods or wind tunnel tests. In this study, the area affected from propeller is defined with mathematical formula, so this brings a freedom about in which angle of attack and tilt angle should be set to use the advantage of propeller effect.

In the transitional flight regime, the dynamics of the vehicle includes the effects as observed at both the hover and the forward-flight regimes. Thus, studies about dynamic modeling of the transition regime mainly focuses on the two fundamental flight regimes (namely hover and forward flight) and blending of these two models through parameterization. In [15], modeling, control and simulation of a tilt-duct UAV is presented. Two – loop state-dependent Riccati Equations (SDRE) control algorithm is applied. Allocating of the controllers during the transition flight is achieved by using blended inverse control allocation algorithm. Specifically the equations of motion of the tilt-duct UAV is described in two flight regimes and the stability analysis is performed based on the linearized equations of motion for trim flight condition. In [16], the authors describe modeling, control and test results of a four tilt-rotor mini-aircraft. For hover flight mode, a nonlinear control algorithm is proposed, consisting of feedback linearization and hierarchical control scheme, is proposed. A Lyapunov-based

backstepping control algorithm is developed for horizontal flight mode. In the follow-up work [17], the authors model the aerodynamic forces in two primary flight regimes and the transition strategy for a control algorithm is defined.

Thus in general, studies on aerodynamic analysis of aircraft are mostly about hover and forward flight regime. However, transitional flight is the most complex case due to flowfield around UAV, rotor/wing interaction, pressure, and force loading throughout the wingspan. In some experimental work [18, 19], different flap deflections were tested to develop rotor/wing interactions, pressure, force loading, and velocity distribution along wingspan. However, in the literature, there is no work on flow-field around aircraft in transition mode using CFD or other numerical methods.

In our approach we focus on modeling the aerodynamics of the transition not as a blend of hover and forward flight aerodynamics but as a standalone effect. Specifically, aerodynamic effects of free airstream and propeller induced airstream are modeled separately by using aerodynamic data which are obtained from CFD analysis. These datasets are used to generate aerodynamic lookup-tables. In addition, aerodynamic coefficients of the airframe are calculated by using CFD method and these data are embedded into the nonlinear model as a lookup-table form. Thrust – flight speed test results of the propeller that are used in tilt-rotor assembly is obtained from the manufacturer's data base and an additional lookup-table is generated for this relationship. In the next section, we review in detail the mathematical modeling associated with all the associated flight regimes.

3 Mathematical Modeling

In this section, we focus on the deriving 6 degree of freedom (DoF) nonlinear mathematical model of the TURAC which includes hover, transition and cruise flight regimes.

3.1 General Equations of Motion

The general equations of motion for the UAV are obtained based on Newton's second law. According to the law of motion, summing all external forces acting on a body is equal to the time derivative of its

momentum with respect to inertial space, as presented mathematically in Eq. 1 [20].

$$\sum \vec{F} = \frac{d}{dt} (m \vec{V}) \quad (1)$$

where F , m , V are force, mass and total speed.

The total moment on a body is defined as the time derivative of its moment of momentum (angular momentum) with respect to the inertial space according to Newton's second law of motion. The mathematical expression of the total moment is shown in Eq. 2 [20].

$$\sum \vec{M} = \frac{d\vec{H}}{dt} \quad (2)$$

where M and H are moment and angular momentum.

Before deriving the nonlinear equations of motion, it is necessary to make following assumptions [21]:

- The XZ plane of the UAV body axis system is the symmetry plane.
- The mass of the UAV remains constant.
- The UAV is a rigid body.
- The earth is the inertial reference.

Defining the axis system as shown from the Fig. 4, body axis system (B) is fixed to the aircraft and inertial axis system (or Earth axis system) (E) is fixed to the Earth.

Using Newton's second law of motion and the above-mentioned assumptions, force and moment equations are derived, as shown in Eqs. 3 and 4. External forces which are placed on the right hand side of the equations, consist of gravity, aerodynamic

and thrust forces. Similarly, external moments are aerodynamic and thrust moments [22].

$$\begin{aligned} m(\dot{U} + QW - RV) &= F_{G_x} + F_{A_x} + F_{T_x} \\ m(\dot{V} + RU - PW) &= F_{G_y} + F_{A_y} + F_{T_y} \\ m(\dot{W} + PV - QU) &= F_{G_z} + F_{A_z} + F_{T_z} \end{aligned} \quad (3)$$

$$\begin{aligned} \dot{P}I_{xx} + QR(I_{zz} - I_{yy}) - (\dot{R} + P Q)I_{xz} &= L_A + L_T \\ \dot{Q}I_{yy} - PR(I_{zz} - I_{xx}) + (P^2 - R^2)I_{xz} &= M_A + M_T \\ \dot{R}I_{zz} + PQ(I_{yy} - I_{xx}) + (QR - \dot{P})I_{xz} &= N_A + N_T \end{aligned} \quad (4)$$

where U , V , W , P , Q and R are linear and angular velocities that defined on the body axis system of the UAV. Gravitational, aerodynamic and thrust effects are defined using G , A , and T subscripts. F , L , M and N denote force, roll moment, pitch moment, and yaw moment, respectively. Inertia moments are denoted using by I_{xx} , I_{yy} , I_{zz} and I_{xz} .

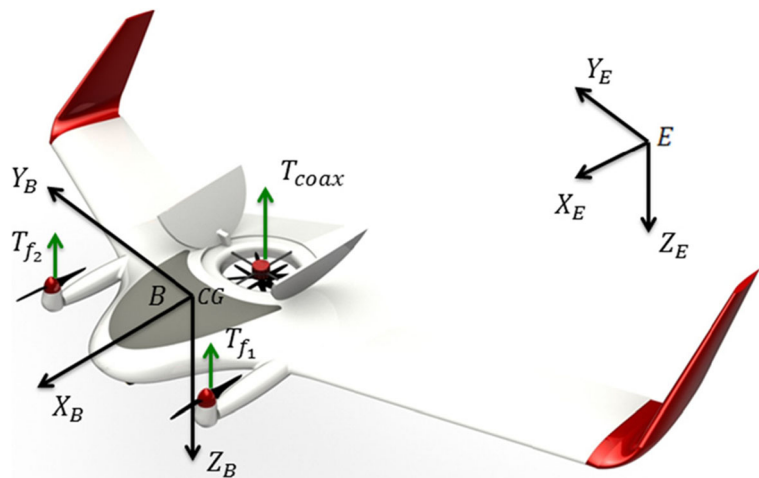
The angular velocity vectors of the UAV are transformed from the Earth axis system to the aircraft body axis system using transformation matrix R , as given in Eq. 5. Body angular velocities are obtained using the R matrix, as shown in Eq. 6.

$$R = \begin{bmatrix} 1 & 0 & -\sin\theta \\ 0 & \cos\phi & \sin\phi\cos\theta \\ 0 & -\sin\phi & \cos\phi\cos\theta \end{bmatrix} \quad (5)$$

$$\begin{bmatrix} P \\ Q \\ R \end{bmatrix} = R \begin{bmatrix} \dot{\phi} \\ \dot{\theta} \\ \dot{\psi} \end{bmatrix} \quad (6)$$

where ϕ , θ , ψ are Euler angles.

Fig. 4 Earth and body axis systems



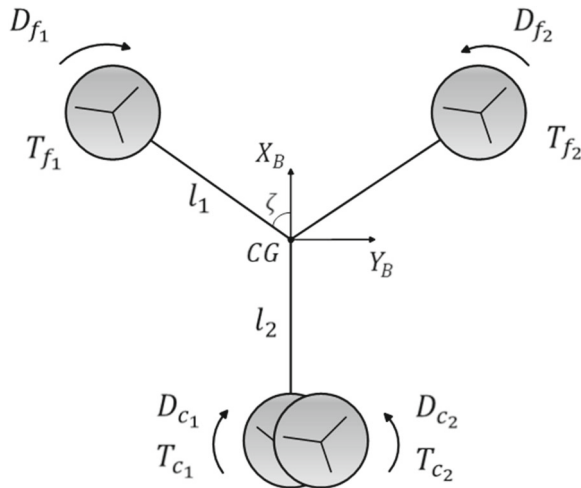


Fig. 5 Force, moment, and some geometrical dimensions of the UAV

The coordinates of the flight path with respect to the Earth axis system are obtained using Eq. 7 as shown below [22].

$$\dot{x}_E = U c \theta c \psi + V (s \phi s \theta c \psi - c \phi s \psi) + W (c \phi s \theta c \psi + s \phi s \psi) \quad (7)$$

$$\dot{y}_E = U c \theta s \psi + V (s \phi s \theta s \psi + c \phi c \psi) + W (c \phi s \theta s \psi - s \phi s \psi)$$

$$\dot{z}_E = -U s \theta + V s \phi c \theta + W c \phi c \theta$$

Here, c and s is symbolize cosine and sine functions, respectively.

3.2 Modeling of Transition Flight

Transition flight is a complex regime between hover and horizontal flight. Forces and moments acting on the UAV body change continuously according to the tilt angle of the front propellers. Before deriving the dynamical equations of the transition flight, it is useful to define some geometrical dimensions, thrust and drag forces that affect the airframe.

In Fig. 5, T_{f1} , T_{f2} , D_{f1} and D_{f2} are thrust forces and drag moments of the tilt-rotor group. T_{c1} , T_{c2} , D_{c1} and D_{c2} are thrust forces and drag moments of the coaxial fan group. l_1 and l_2 are moment arms, ζ is the angle between l_1 and X_B axis. In [2, 4], a detailed description of motor-propeller configuration and performance test results are given.

In the hover regime, there is no aerodynamic force or moment acting on the UAV body because of the absence of the forward airspeed. When the front motors start to rotate about the tilting axis, horizontal force is created proportional to the tilting angle. So, aerodynamic lift force, drag force, and pitching moment affect the airframe, as shown in Fig. 6.

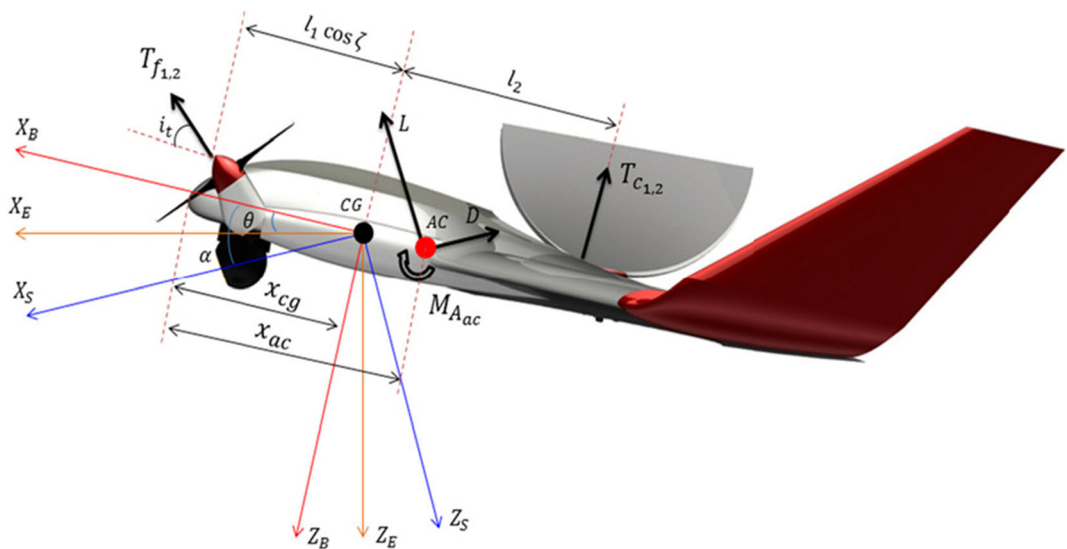


Fig. 6 Forces and moments on the TURAC in transition flight

Six-degree-of-freedom equations of motion can be rewritten as shown in Eqs. 8 and 9.

$$\begin{aligned} m(\dot{U} + QW - RV) &= -mgs\theta + (-Dc\alpha + Ls\alpha) \\ &\quad + (T_{f1} + T_{f2})ci_t \end{aligned}$$

$$m(\dot{V} + RU - PW) = F_{G_y} + F_{A_y} + F_{T_y} \quad (8)$$

$$\begin{aligned} m(\dot{W} + PV - QU) &= mgc\phi c\theta \\ &\quad + (-Ds\alpha - Lc\alpha) \\ &\quad - ((T_{f1} + T_{f2})si_t + T_c) \end{aligned}$$

$$\begin{aligned} \dot{P}I_{xx} + QR(I_{zz} - I_{yy}) - (\dot{R} + PQ)I_{xz} \\ = L_A + (T_{f1} + T_{f2})l_1s\xi \end{aligned}$$

$$\begin{aligned} \dot{Q}I_{yy} - PR(I_{zz} - I_{xx}) + (P^2 - R^2)I_{xz} \\ = (M_{A_{fs}} + M_{A_p}) - (Lc\alpha + Ds\alpha)(x_{ac} - x_{cg}) \\ + ((T_{f1} + T_{f2})l_1si_t c\xi - T_c l_2) \quad (9) \end{aligned}$$

$$\begin{aligned} \dot{R}I_{zz} + PQ(I_{yy} - I_{xx}) + (QR - \dot{P})I_{xz} \\ = N_A + (D_{f1} + D_{f2} + D_{c1} + D_{c2}) \end{aligned}$$

3.3 Propeller-Induced Airflow Effects

In the previous subsection, it is explained that, the forces and moments on the UAV are created by the

thrust system and the airflow that passes through the body.

Aerodynamic forces and moments exerted on the UAV are functions of total airflow vector, V_T . So, it is important to determine the magnitude and direction of the total airflow.

As shown in Fig. 7, there are two separate airflow vectors acting on the UAV. The first one is V_∞ which is defined as free airstream velocity and it is generated by translational motion. The second one is V_∞ and it is generated by translational motion. The components of V_∞ are body axis velocity vectors U and W . The second airflow vector acting on the body is propeller-induced airflow V_{out} . It is a function of front propeller thrust $T_{f1,2}$, air density ρ , propeller area A and intake airflow velocity of the propeller V_{in} .

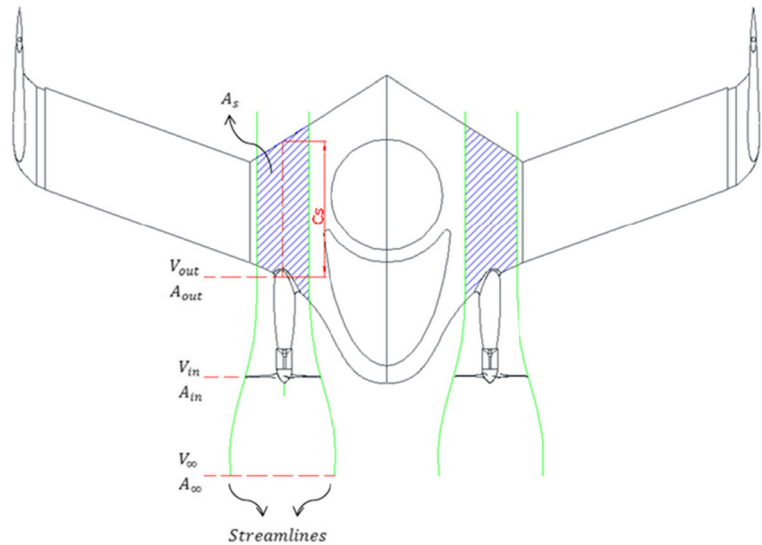
Input and output velocities of the propeller are shown in Fig. 7. These velocities are calculated using classical momentum theory as shown in Eqs. 10 and 11:

$$V_{in} = \frac{V_\infty \cos \alpha \cos i_T + V_{out}}{2} \quad (10)$$

$$V_{out} = \sqrt{\frac{2T_f}{\rho \pi R_p^2} + (V_\infty \cos \alpha \cos i_T)^2} \quad (11)$$

In Eq. 10, intake airflow velocity V_{in} is defined in the term of tilt angle and angle of attack which is an important detail for transition scenario calculations. Note that Eqs. 10 and 11, appear differently than their

Fig. 7 Propeller induced airflow effects on the UAV body



form in momentum theory, and these are due to angle of attack and tilt angle.

According to the continuity equation, output cross-section area of the propeller induced airflow changes as a function of V_{in} and V_{out} :

$$A_{out} = \frac{\pi R_p^2 V_{in}}{V_{out}} \quad (12)$$

In transitional and horizontal flight, the total airflow vector flows over in a specific area (A_s) on the UAV body as shown in Fig. 7 and it is calculated geometrically as given in Eq. 13.

$$A_s = 2R_s c_s \quad (13)$$

where c_s is mean aerodynamic chord of the specified region that shown in Fig. 7.

In hover flight, the thrust axis of the tilt rotors is perpendicular to the X_B axis, so any propeller-induced aerodynamic effects are not observed on the body. When the tilt angle starts to decrease, additional forces and moments are generated due to the propeller airstream. However, this effect does not occur suddenly. It changes step-by-step as a function of tilt angle. For this type of change, an effectiveness coefficient ξ is defined as an assumption in modeling the tilt-rotor aerodynamic effect on the UAV body. We model it as a sigmoid function as shown in Eq. 14. In Fig. 8, the change of effectiveness coefficient is shown as a function of tilt angle.

$$\xi = 1 - \frac{1}{1 + e^{-0.15(i_t - 45)}} \text{ for } \xi \in [1, 0] \quad (14)$$

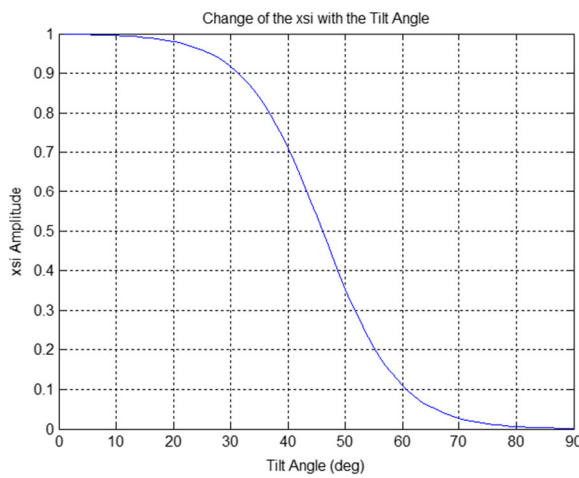


Fig. 8 Change of effectiveness coefficient with the tilt angle

The effectiveness coefficient ξ is used to calculate the total effective velocity on the body profile while the tilt angle value is between 0 and 90 degrees.

3.3.1 Free Airflow Effects

The free airflow passes through from the area which is not affected by the propeller-induced airflow. In the beginning of transition flight regime, the effect of the free airflow is dominant on the UAV because of the almost-vertical tilt-rotors. So, it is important to represent the aerodynamic effect of this airflow vector.

The aerodynamic forces (L_w, D_w, Y_w) and moments (m_w, l_w, n_w) of the UAV without propeller effect are calculated in Eq. 15. In the following equations, the region which is not affected by the propeller-induced airflow is specified as ($A - 2A_s$)

$$\begin{aligned} L_w &= \bar{q}(A - 2A_s)C_{Lw} \\ D_w &= \bar{q}(A - 2A_s)C_{Dw} \\ Y_w &= \bar{q}(A - 2A_s)C_{Yw} \\ m_w &= \bar{q}(A - 2A_s)\bar{c}C_{mw} \\ l_w &= \bar{q}(A - 2A_s)bC_{lw} \\ n_w &= \bar{q}(A - 2A_s)bC_{nw} \end{aligned} \quad (15)$$

where A is the planform area of the UAV and \bar{q} is dynamic pressure. Here, w subscript is used to represent the free airflow forces and moments. Aerodynamic coefficients in Eq. 15 are derived as shown in Eq. 16.

$$\begin{aligned} C_{Lw} &= C_{Lw,b} + C_{Lw\delta_e}\delta_e + C_{L\dot{\alpha}}\frac{\dot{\alpha}\bar{c}}{2U_1} + C_{Lq}\frac{q\bar{c}}{2U_1} \\ C_{Dw} &= C_{Dw,b} + C_{Dw\delta_e}\delta_e + C_{D\dot{\alpha}}\frac{\dot{\alpha}\bar{c}}{2U_1} + C_{Dq}\frac{q\bar{c}}{2U_1} \\ C_{mw} &= C_{mw,b} + C_{mw\delta_e}\delta_e + C_{m\dot{\alpha}}\frac{\dot{\alpha}\bar{c}}{2U_1} + C_{mq}\frac{q\bar{c}}{2U_1} \\ C_l &= C_{l_{w,b}} + C_{l_{\delta_a}}\delta_a + C_{l_{\delta_r}}\delta_r + C_{lp}\frac{pb}{2U_1} + C_{lr}\frac{rb}{2U_1} \\ C_Y &= C_{Y_{w,b}} + C_{Y_{\delta_a}}\delta_a + C_{Y_{\delta_r}}\delta_r \\ &\quad + C_{Yp}\frac{pb}{2U_1} + C_{Yr}\frac{rb}{2U_1} \\ C_n &= C_{n_{w,b}} + C_{n_{\delta_a}}\delta_a + C_{n_{\delta_r}}\delta_r \\ &\quad + C_{np}\frac{pb}{2U_1} + C_{nr}\frac{rb}{2U_1} \end{aligned} \quad (16)$$

where;

$$\begin{aligned} C_{L_{w,b}} &= C_{L_0} + C_{L_\alpha} \alpha \\ C_{D_{w,b}} &= C_{D_0} + C_{D_\alpha} \alpha \\ C_{m_{w,b}} &= C_{m_0} + C_{m_\alpha} \alpha \\ C_{Y_{w,b}} &= C_{Y_0} + C_{Y_\beta} \beta \\ C_{l_{w,b}} &= C_{l_0} + C_{l_\beta} \beta \\ C_{n_{w,b}} &= C_{n_0} + C_{n_\beta} \beta \end{aligned}$$

Here, the aerodynamic coefficients with (*wb*) subscript represents the wing-body geometry effects on each coefficient.

In transition flight, longitudinal aerodynamic coefficients of the wing-body geometry identify the dynamic characteristics of the UAV. So, $C_{L_{w,b}}$, $C_{D_{w,b}}$ and $C_{m_{w,b}}$ are obtained by using 3D CFD analysis. They are used to generate lookup-tables which is embedded into the nonlinear mathematical model. Remaining aerodynamic coefficients, including lateral directional coefficients, are obtained by using Advanced Aircraft Analysis (AAA) software. During our analysis, we assume that the aerodynamic coefficients of the UAV body (i.e. the part which is carrying the payload and the avionics) are not affected by coaxial fan airstream. Thus in this sense, we are assuming the lift and drag coefficients to be constant for the body part. This is indeed a valid approach as the wing is the preliminary force generation mechanism. This is further illustrated and verified by the CFD analysis

3.3.2 Total Airflow Effects

In transition flight, there are very complex and nonlinear aerodynamic effects on the UAV which are created by the free and propeller induced airflows. So, it is very hard to represent these nonlinear aerodynamic effects mathematically without making any assumptions.

In this study, free and propeller-induced airflow effects are modeled linearly by using superposition rule. Hence, these two aerodynamic effects are examined separately. This assumption essentially simplifies the derivation of the mathematical representations. For this purpose, the lift force, drag force and pitching moment are calculated for two situations as with propeller effect (L_s , D_s , M_s) and without propeller effect (L_w , D_w , M_w). Then, the values of aerodynamic forces and moments with and without propeller

effect are summed up to obtain the total aerodynamic effects on the UAV body.

Both the free airstream and the propeller-induced airstream are effective on A_s . Therefore, the total airspeed (V_T) is used to calculate the lift force, drag force and pitching moment that generated on A_s as shown in Eq. 17.

$$\begin{aligned} L_s &= \frac{1}{2} \rho V_T^2 A_s C_{L_s} \\ D_s &= \frac{1}{2} \rho V_T^2 A_s C_{D_s} \\ M_s &= \frac{1}{2} \rho V_T^2 A_s c_s C_{M_s} \end{aligned} \quad (17)$$

As shown from the Fig. 7, there is no downwash effect on the section that the propeller induced airstream passes through. So, this region can be assumed as infinite wing. Hence, the aerodynamic coefficients in Eq. 17 are obtained from 2D analysis of the wing airfoil and lookup-tables are generated. The detail information about this subject is given in the CFD analysis section.

The total airspeed that affects the above-mentioned area A_s is defined in vector form as shown in Fig. 9 and it is calculated by using Eq. 18.

$$V_T = \sqrt{(V_{out} \xi \sin(\alpha + i_t))^2 + (V_{out} \xi \cos(\alpha + i_t) + V_\infty)^2} \quad (18)$$

The airflow over the wing is affected by freestream velocity and output velocity of the propeller. Propeller-induced airstream velocity is separated into its x and y components, because of inserting freestream velocity as shown in Eq. 18. Tilt effect is also shown in calculation as tilt angle (i_t) in this equation.

As mentioned before, the total airflow vector V_T passes through the specified area A_s on the UAV body. Magnitude of the V_T is a function of freestream airflow speed, angle of attack and tilt angle. For modeling of aerodynamic effects of the total airflow vector, it is important to define effective angle of attack α_{eff} on the A_s which is produced by propeller-induced airstream and free airstream vectors. Geometrically, α_{eff} is calculated by using Eq. 19.

$$\alpha_{eff} = \arctan \left(\frac{V_\infty \sin \alpha - V_{out} \sin i_t}{V_\infty \cos \alpha + V_{out} \cos i_t} \right) \quad (19)$$

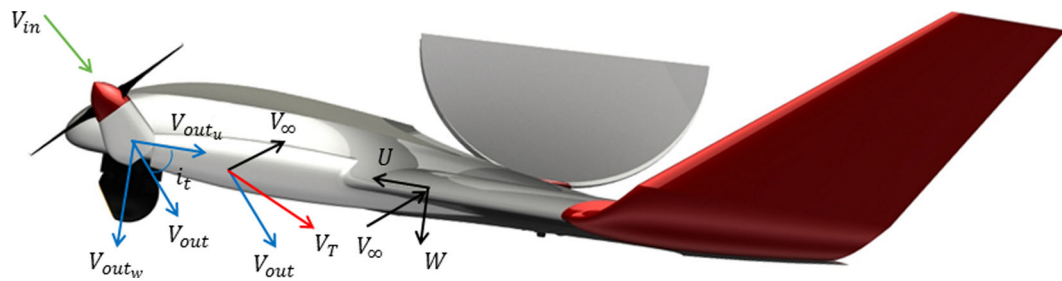


Fig. 9 Total airspeed vector

Unlike propeller effect on a conventional airplane wing, tilt angle is inserted into the tilt-rotor calculations of effective angle of attack in VTOL concept.

3.4 Modeling the Thrust-Flight Speed Relationship for the Tilt-Rotor Propeller

Propeller intake airflow speed (V_{in}) is the freestream velocity which is in the same direction as propeller rotation axis. The value of V_{in} and thrust relate to the angle of attack and the tilt angle. In other words, the angle of attack on the propeller blades decreases as the intake airflow speed increases. So, thrust decreases because of the low angle of attack on the blades.

In Fig. 10, propeller intake airflow speed—generated thrust characteristics of the 12x6 inch fixed-pitch propeller are shown for various RPM. The test data for different airspeed and RPM are available at producer's database. This dataset is used to generate

thrust functions and lookup-tables with respect to airspeed for each RPM. A surface function is used to find out thrust forces at different airspeed which is not available at the test data.

3.5 Computational Fluid Dynamics Analysis

Computational Fluid Dynamics (CFD) is used to generate aerodynamic coefficients and create transition and back-transition scenarios. The 2D-analysis of the wing airfoil is used to develop the transition scenario. In this section, 2D analysis, forward flight, and transition flight are explained.

3.5.1 2D Airfoil Analysis

As mentioned before, the propeller induced airflow passes through the wing profile and there is no finite-wing effects (See Fig. 7). So, this region is assumed

Fig. 10 Thrust - propeller intake airflow speed characteristics of the 12x6 fixed-pitch propeller

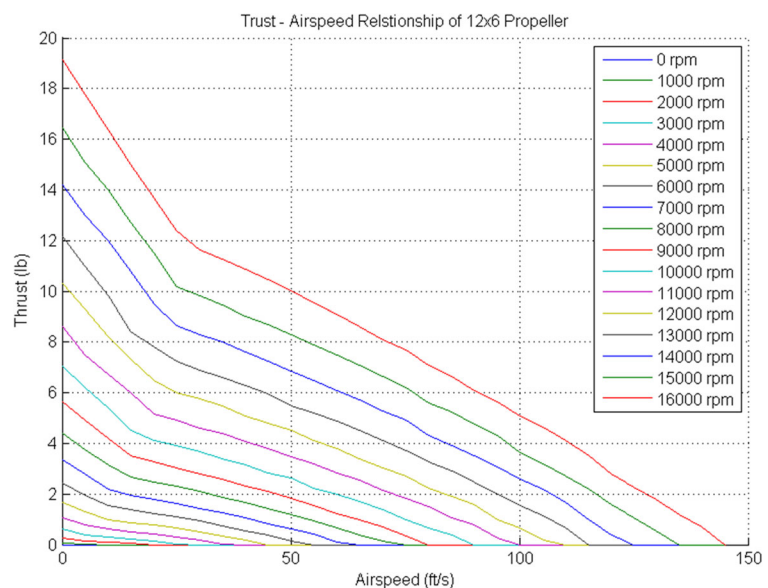
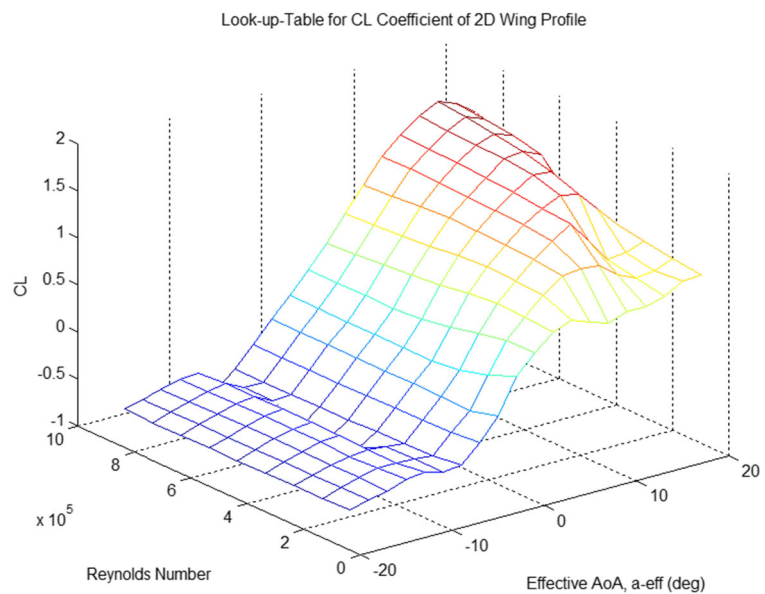


Fig. 11 Lift coefficient (C_{L_s}) of the 2D wing airfoil for different Reynold numbers



as infinite wing and 2D aerodynamic analysis can be used to calculate the aerodynamic coefficients of this region.

The wing airfoil of TURAC is selected as MH-78 and its aerodynamic coefficients are calculated by using 2D analysis for different Reynold numbers in XFLR5 which applies Vortex Lattice Method (VLM). The lift coefficient (C_{L_s}) of wing profile at 2D analysis versus Reynolds number and elevator angle is shown in Fig. 11. Similarly, in Figs. 12 and 13, the drag coefficient (C_{D_s}) and the drag coefficient (C_{M_s})

of wing profile versus Reynolds number and elevator angle is shown.

3.5.2 3D CFD Analysis

The CFD analysis for forward and transition flights is done in four steps: creating model and control volume, meshing whole geometry, building up boundary layer and setting up the analysis. In this study, the cases are prepared for forward and transition flight step by step to solve the problem accurately. One of the important

Fig. 12 Drag coefficient (C_{D_s}) of the 2D wing airfoil for different Reynold numbers

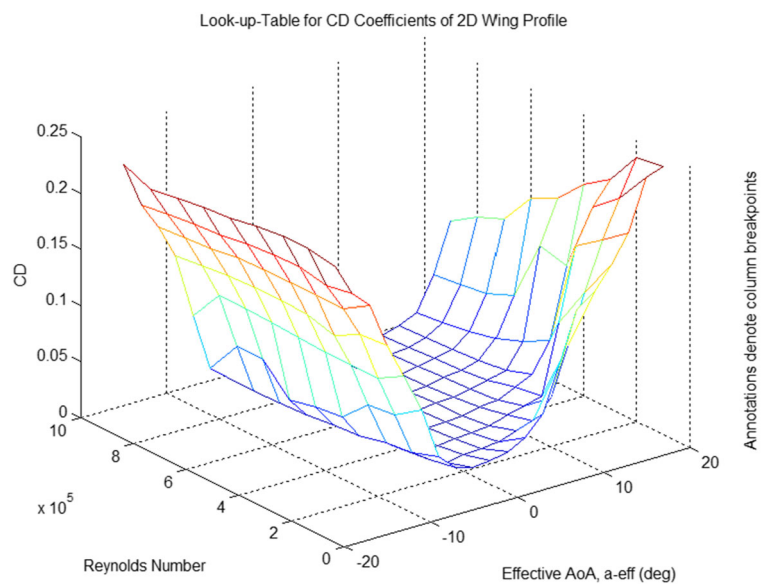
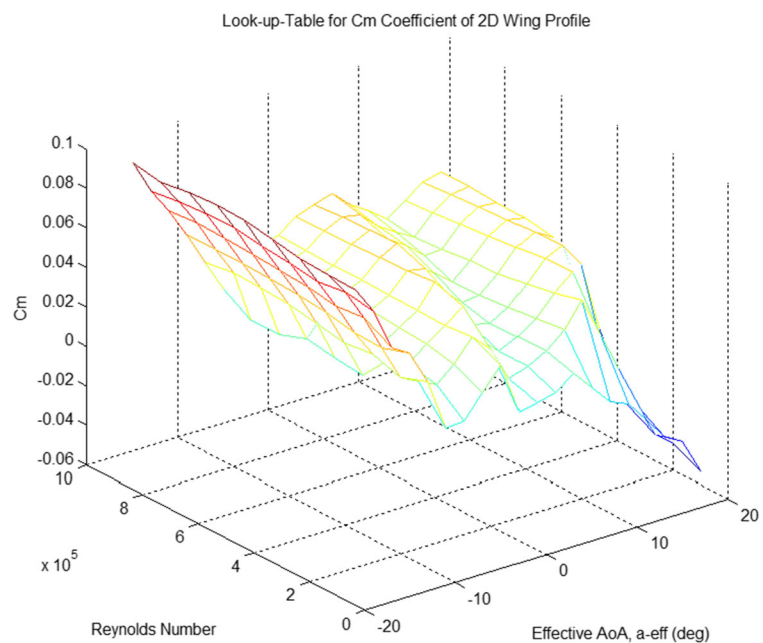


Fig. 13 Pitching moment coefficient (C_{m_2}) of the 2D wing airfoil for different Reynolds numbers



issues in the analysis is generating boundary layers with respect to the value of $y+$ which is 1 for the first cell height of the boundary layer. The value of $y+$ changes due to viscous, transition and turbulence regime. It is a vital issue for the quality of the analysis.

In the analysis, Fluent is used as a solver program. The K-epsilon Realizable Enhanced Wall Treatment turbulent model is obtained for all CFD cases.

In developing part of the transition and back transition scenarios, aerodynamic coefficients are provided from the CFD analysis. In these analysis, half of TURAC is modeled because of symmetry to decrease solving time memory use. For the analysis, the coaxial fan door is closed as in forward flight. The model of the half TURAC can be seen in Fig. 14. It is

lied on one of the control volume wall which is set as symmetry.

The half of TURAC geometry at forward flight concept is analyzed from 0° to 15° angle of attack at forward flight speed. The aerodynamic coefficients are calculated from the mentioned analysis. Moreover, the same analysis for different forward flight speed at the constant angle of attack are repeated to search the change of aerodynamic coefficients. The analysis are applied for -3° , 0° and 3° angle of attack values at 5 m/s, 10 m/s, 15 m/s and 20 m/s forward flight velocities. Table 2 shows the aerodynamic coefficients of TURAC due to different forward flight speed at constant angle of attack. In that sense, we assume that the aerodynamic coefficients of the TURAC prototype do not change with respect to airspeed.

Fig. 14 The half of TURAC model for forward flight regime in CFD analysis

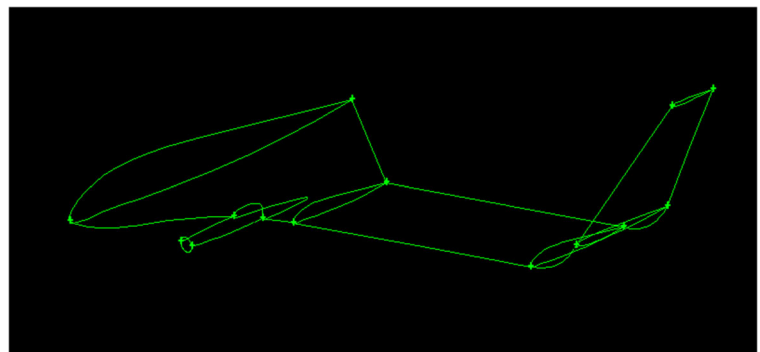


Table 2 The force and moment coefficient for transition scenario

$\alpha(^{\circ})$	$V(m/s)$	C_L	C_D	C_M
-3	15	-0.08601	0.04092	0.01516
	20	-0.08699	0.03964	0.01589
0	5	0.12406	0.03836	-0.09538
	10	0.12376	0.03489	-0.09486
	15	0.12496	0.03321	-0.09521
	20	0.12494	0.03209	-0.09499
	3	0.34476	0.04104	-0.20825
3	10	0.3468	0.03745	-0.20864
	15	0.34844	0.03567	-0.20921
	20	0.34927	0.0345	-0.20926

In Table 2, as the angle of attack increases, lift and drag coefficients increase and pitching moment coefficient decreases. It can be seen obviously in the table that the aerodynamic coefficients do not change with the Reynolds number at constant angle of attack.

In Fig. 15, the change of pressure on the TURAC can be seen. The values of static pressure on the colorbar are Pascal. The highest value of pressure is at the nose and tilt component. The lowest pressure on TURAC is at the quad-chord of the wings.

In the nonlinear mathematical model of the TURAC, it is necessary to generate the lookup-tables represent the aerodynamic effects of the wing-body

geometry. For this purpose, the 3D CFD dataset is obtained for forward flight in $0^{\circ} - 15^{\circ}$ angle of attack region which includes stall effects as shown in Figs. 16, 17 and 18.

The same aerodynamic coefficients were used at different forward flight velocities for calculations of transition and back-transition scenarios, as per the description and Table 2.

A part of the transition scenario is also modeled and analyzed by using CFD method. Further information on the the transition-flight analysis can be found in [1]. In this model complete TURAC is used and two tilt propellers and coaxial propellers are modeled as fan

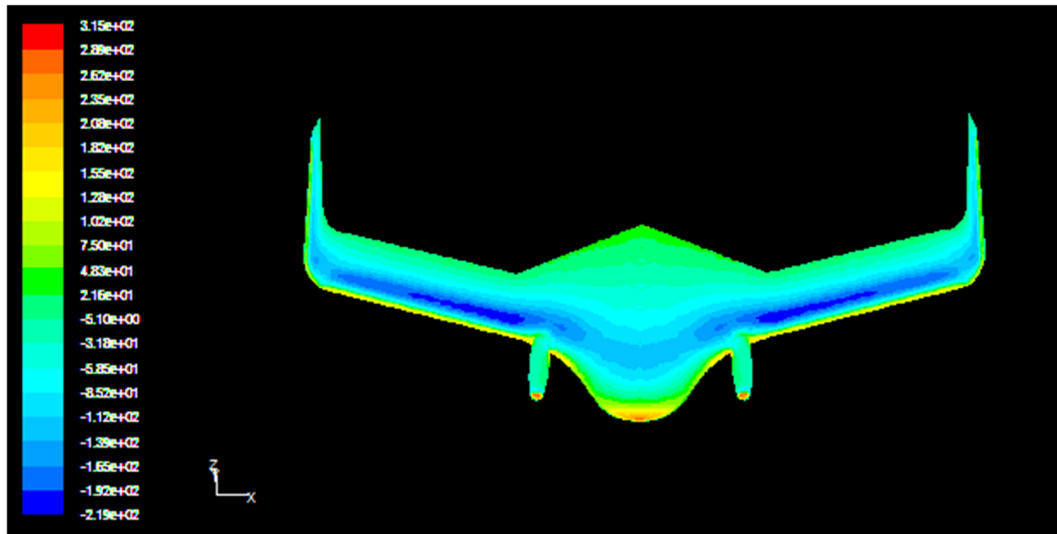
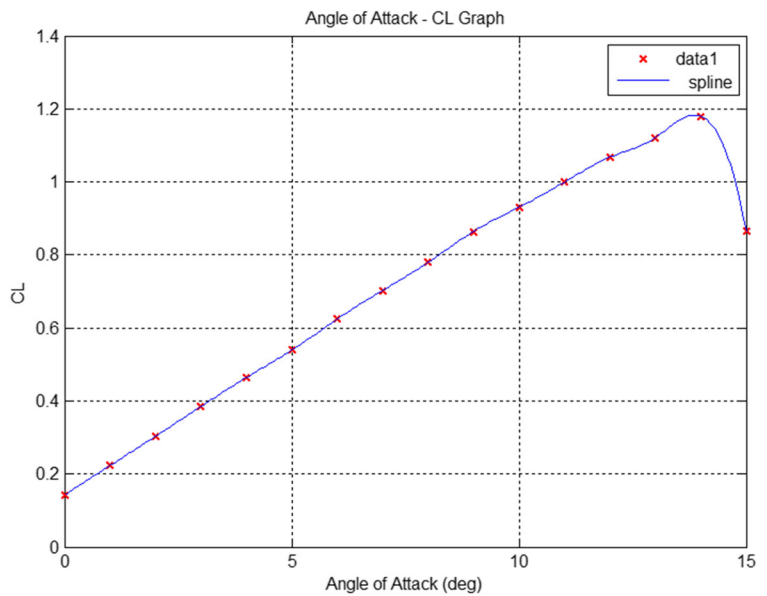


Fig. 15 The static pressure distribution of TURAC

Fig. 16 Angle of attack - C_L graph of the TURAC



boundary condition. In this analysis, coaxial part of the TURAC is open because of the transition concept. As boundary conditions for propeller, a pressure jump is inserted in order to properly define the thrust produced by each propeller. The pressure jump of the propeller is calculated from momentum theory. Figure 19 shows the streamlines of the TURAC at 70° tilt angle and -1° angle of attack at 10 m/s forward flight speed.

In Fig. 19, the flow is inserted into the propeller disc for tilt and for coaxial rotors. The swirl of the flow can also be seen in the figure behind the propellers. The streamlines on the wings are smooth compared to those on the body. The body of TURAC has airfoil profile which produces lift during forward flight. However, in transition flight, the contribution of body in producing lift is very poor because of the complex

Fig. 17 Angle of attack - C_D graph of the TURAC

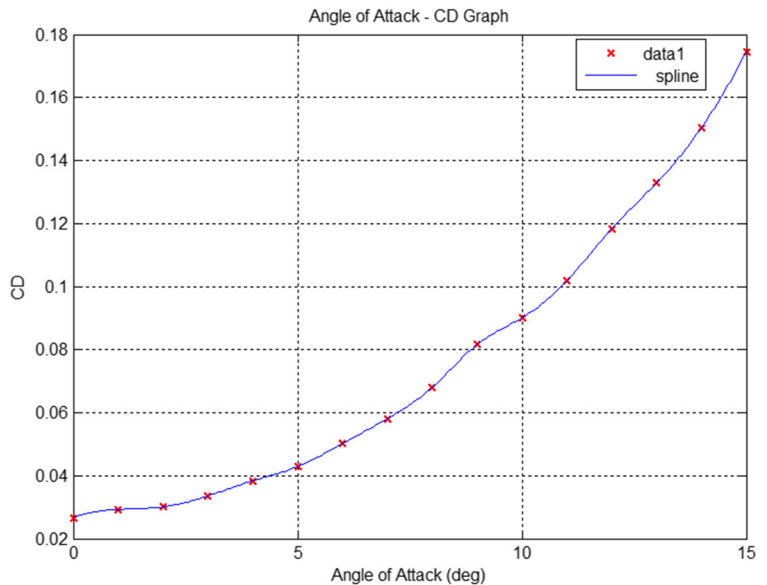
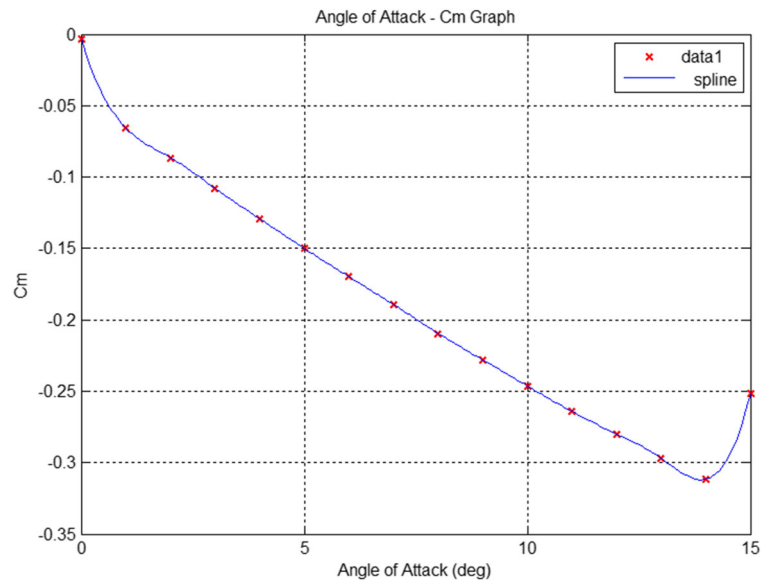


Fig. 18 Angle of attack - C_m graph of the TURAC



flow on the body and the opened fan doors. For this reason, we assume the lift and drag contribution of the body to be independent of the coaxial fan operation during the hover and the transition.

In Fig. 20, the static distribution on TURAC body can be seen. According to these results, the aerodynamics of the transition regime is extremely complex. However it is apparent that the forces and moments generated by the tilt and the coaxial propellers and the net force effects are extremely important in defining the transition regime and maneuver. In the next subsection we drive the thrust forces necessary to achieve

a balanced transition (both in forces and moments) for a designed transition scenario.

3.6 Transition Scenario

As to achieve a balanced transition from hover to forward flight (and vice versa), it would be necessary to drive the necessary the magnitude of forces for both the tilt-rotors and lifting fan. Through the application of these forces during the transition, one would ensure a balanced transition into the forward flight (or hover). The total force in the x and z directions and moment

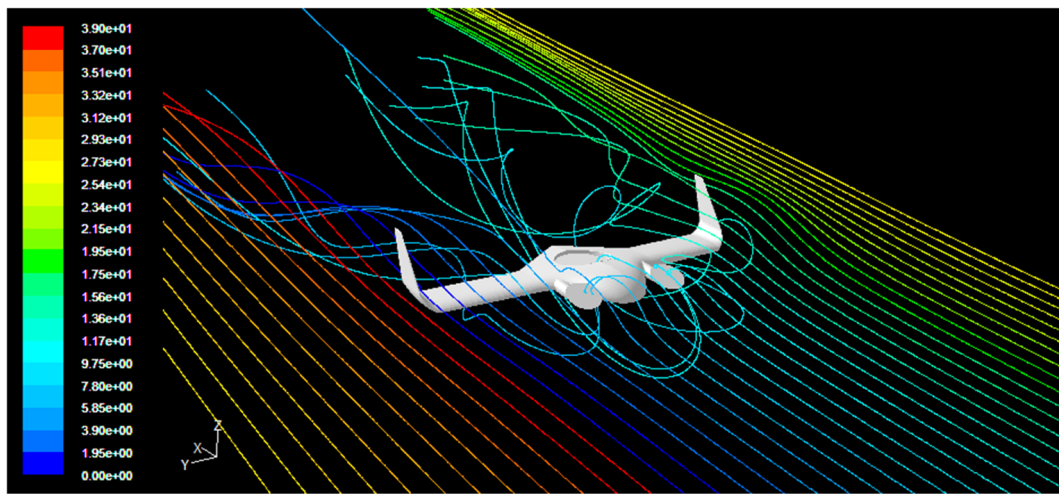


Fig. 19 The pathlines of TURAC in transition regime

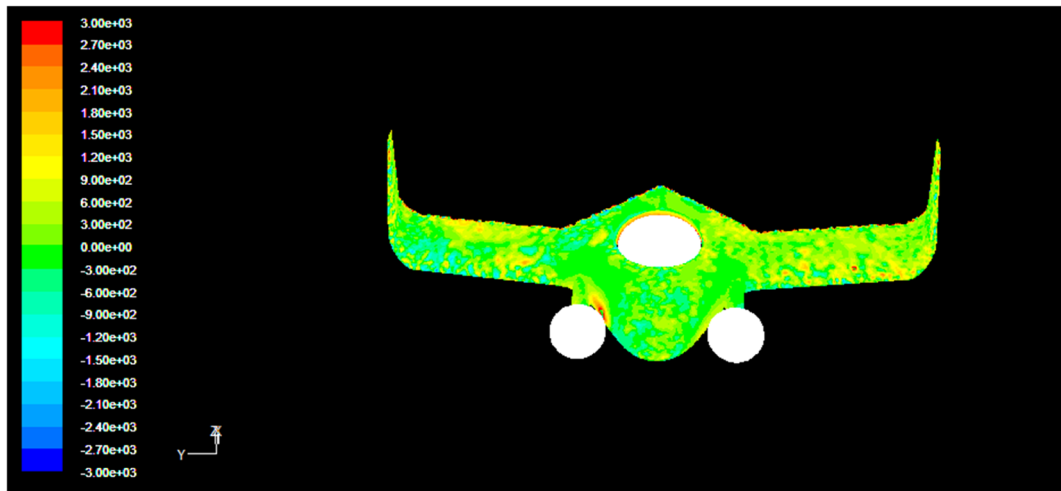


Fig. 20 The static pressure distribution of TURAC in transition regime

around aerodynamic center can be calculated using Eq. 20:

$$\begin{aligned}
 F_z &= L_w \cos a + 2T(\sin i_T)(\cos a) + L_s \cos(a_w) \\
 &\quad - D_s \sin(a_w) + T_{coax} \cos a - W \\
 F_x &= 2T(\cos i_T)(\cos a) - D_w - L_s \sin(a_w) \\
 &\quad - D_s \cos(a_w) - T_{coax} \sin a \\
 M_{ac} &= 2Tsini_T(x_{AC} - x_T) + T_{coax}(x_{AC} - x_{T_{coax}}) \\
 &\quad + +W(x_{AC} - x_W) \cos a
 \end{aligned} \tag{20}$$

Here positive direction is lift direction at $\sum F_z$ and thrust direction at $\sum F_x$ [23]. The pitching moment coefficient is obtained using Eq. 21:

$$C_M = \frac{M_{ac}}{\frac{1}{2}\rho V^2 c S} + C_{M_{de}} \delta_e \tag{21}$$

Using the force descriptions, a transition scenario is developed for the 1/3 scale TURAC prototype. In the designed transition scenario, which is shown in Table 3, excess thrusts are produced at each step of the transition as to accelerate the UAV. In this scenario, the speed of the UAV increases almost uniformly during the transition flight regime. At the last step of transition, all aerodynamic forces and moment equal to zero to achieve forward flight trim equilibrium point.

At the transition flight regime first, the front tiltrotor propeller angle is set as 70° and angle of attack

Table 3 The force and moment coefficient for the third scenario

V	i_T (°)	α (°)	T_f (N)	T_{coax} (N)	$\sum F_x$	$\sum F_z$	C_M
2	70	-1	8.58	39.29	7.44	-0.086	-0.0015
5	70	-1	8.59	39.38	7.5	-0.005	-0.002
10	70	-1	8.55	39.2	7.44	0.066	-0.001
15	70	-1	8.55	38.68	7.28	-0.001	0.002
20	70	-1	8.7	37.76	7.13	0	0.006
25	70	-1	10.2	29.86	7.82	0.006	-0.001
29	70	-1	19.8	0	14.9	0.002	0.049
32	0	0.5	24.9	0	44.5	0	-0.005
35	0	0.5	3	0	-0.005	0.005	0.021
40	0	0.5	3.9	0	-0.043	-0.061	0.075

Table 4 The force and moment coefficient for back transition scenario

V	$i_T(\circ)$	$\alpha(\circ)$	$T_f(N)$	$T_{coax}(N)$	$\sum F_x$	$\sum F_z$	C_M
40	90	0.5	0.8	0.47	-10.1	-0.019	0.0377
35	90	0.5	1.2	1.5	-7.84	-0.009	-0.0044
32	90	0.5	3.21	5.85	-6.9	0.006	0.0012
29	90	0.5	4.2	11.5	-5.88	0.019	0.0004
25	90	0	7	22	-3.56	-0.01	0.0071
20	90	0	7.44	28	-2.26	-0.002	0
15	90	0	8.1	32	-1.26	-0.009	-0.0034
10	90	0	8.6	35	-0.55	0.002	-0.0048
5	90	0	9	36.5	-0.12	0.059	0.0003
2	90	0	9.15	36.7	0.003	-0.004	-0.0037

at -1° until 29 m/s forward flight speed. The scenario continues until 40 m/s in order to establish stable forward flight after the transition flight regime. The aerodynamic forces and pitching moment are calculated for each flight speed by using the above-mentioned equations.

Here the coaxial fan force and the tilt rotor forces are calculated to achieve almost perfect balanced flight in z force direction and around y moment direction. In addition, the elevator angle δ_e was also used in order to have balanced and stable flight throughout the complete transition regime. Elevator angle (δ_e) is set as 0° until 20 m/s, then it equals 6.45° at 25 m/s, 17° at 29 m/s, -1° at 32 m/s, -5.548° at 35 m/s and -15° at 40 m/s. In the scenario, excess thrust occurs until 32 m/s to accelerate the UAV in x direction, then the balance situation is provided after that speed. Thrust produced by the coaxial engine starts from a high value and decreases to zero. In complete scenario, moment coefficient and $\sum F_z$ almost equals to zero and thus in perfect z-force and y-moment balance. Also note that in the last two steps of the scenario, all aerodynamic forces and pitching moment are zero which means the UAV is at equilibrium at cruise speed.

The back-transition scenario is also developed from forward flight regime to hover flight as shown in Table 4. In back transition regime, the thrust of the tilt and coaxial engines are increased as the forward flight velocity decreases. At the last step, lift and drag forces and pitching moment equal to zero to make the UAV in balance.

In this scenario, the tilt angle is set at 90° during whole scenario. The back-transition scenario is the inverse of the transition scenario. It starts at 40 m/s forward flight with 90° tilt angle, then the UAV slows

down by changing the thrust of tilt and coaxial angle, angle of attack and elevator deflection (δ_e).

In this scenario, elevator angle (δ_e) is not set to 0° from start. It is set to -7.42° at 40 m/s, -1.6° at 10 m/s, -6° at 5 m/s and -2.8° at 2 m/s. The thrust of the tilt and coaxial engines start from almost zero and increase until reaching the values of hover-flight thrust. At 2 m/s airspeed, aerodynamic forces and moment are at zero which means the UAV is at equilibrium and in full hover regime.

In the next section, we show the design of a transition control system which uses the provided hover to forward flight and forward to hover flight transition scenarios as feedforward signals. In addition we provide the details of a complete flight which involves hover-forward flight-hover regimes demonstrating fully controlled flight envelope.

4 Complete Mathematical Model and Simulations

In Section 3, we had presented the thrust and aerodynamic effects and showed the highly nonlinear relations that govern not only the hover, forward flight but also the transition flight regime. Combining the dynamics associated with hover, transition and forward flight in Fig. 21, we obtain the general block diagram of the nonlinear mathematical model of the complete flight envelope. Here the flight controls for each of the regimes are also represented with switching functions between each of these regimes.

To demonstrate the feasibility of the transition control scheme in experiment, we have designed a control system a readily (and easily) implementable PID structured and cascaded control system. The cascade

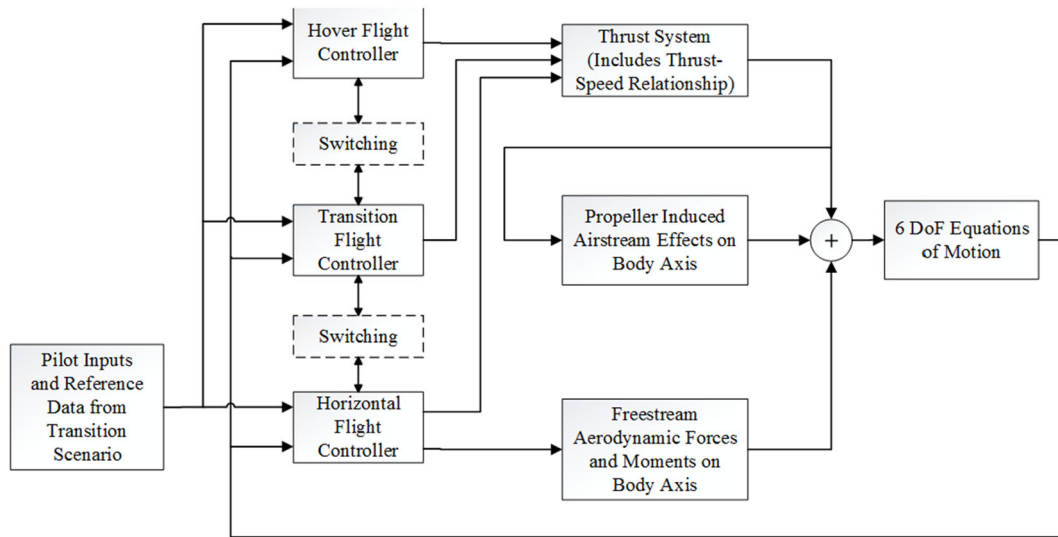


Fig. 21 General block diagram of the nonlinear mathematical model of the complete flight regimes

control system consists of a three-loop PID controller. In these control systems, rate feedback is performed in the first loop to increase the stability. Then, attitude data is fed back into the second loop to generate reference attitude commands. In the third loop, linear velocity is fed back into to the controller. Beside the hover and transition control systems, horizontal flight control system contains classical attitude controllers such as roll, pitch and yaw control systems which are also designed based on PID control.

4.0.1 Transition and Back-Transition Algorithms

In Section 3, detailed transition and back-transition scenarios are obtained by using basic force and moment equations. Before applying these scenario dataset into the nonlinear mathematical model as a reference signal, it is important to sequence the algorithm that is used for switching between low-level controllers. Transition and back-transition algorithms are shown in Fig. 22. High-level flight control system is programmed according to these algorithms.

Following Fig. 22, Step-by-step transition algorithm is described as following;

1. TURAC is in hover flight regime. Tilt-rotors are positioned vertically and three-loop hover controller runs to track linear velocity commands ($V_{ref,hover} < 3m/s$) in hover flight.

2. Acceleration in hover regime up to $3m/s$ flight speed. Step 1 and Step 2 are coded as Phase 1.
3. If the flight speed V_∞ reaches to $2m/s$, the transition controller is activated and the tilt-rotors are positioned at 80°
4. Acceleration in transition regime up to $25m/s$ flight speed. Step 3 and Step 4 are coded as Phase 2.
5. If the flight speed V_∞ reaches to $25m/s$, the horizontal flight controllers are activated and the tilt-rotors are positioned at 0° . Horizontal flight regime is coded as Phase 3.

Step-by-step back-transition algorithm is described as following;

1. It is important to reduce the flight speed before transition regime. To do this, the front propellers are stopped and the aircraft starts to glide.
2. If the flight velocity is lower than $25m/s$, the transition controller is activated.
3. Tilt angle is positioned at 90°
4. Pitch up command is send to the system to decelerate until the $3m/s$ flight speed.
5. Hover controller is activated and TURAC flies in hover regime.

4.0.2 Simulations Results

In this part of study, simulations are performed on 6-DoF nonlinear mathematical model and a complete

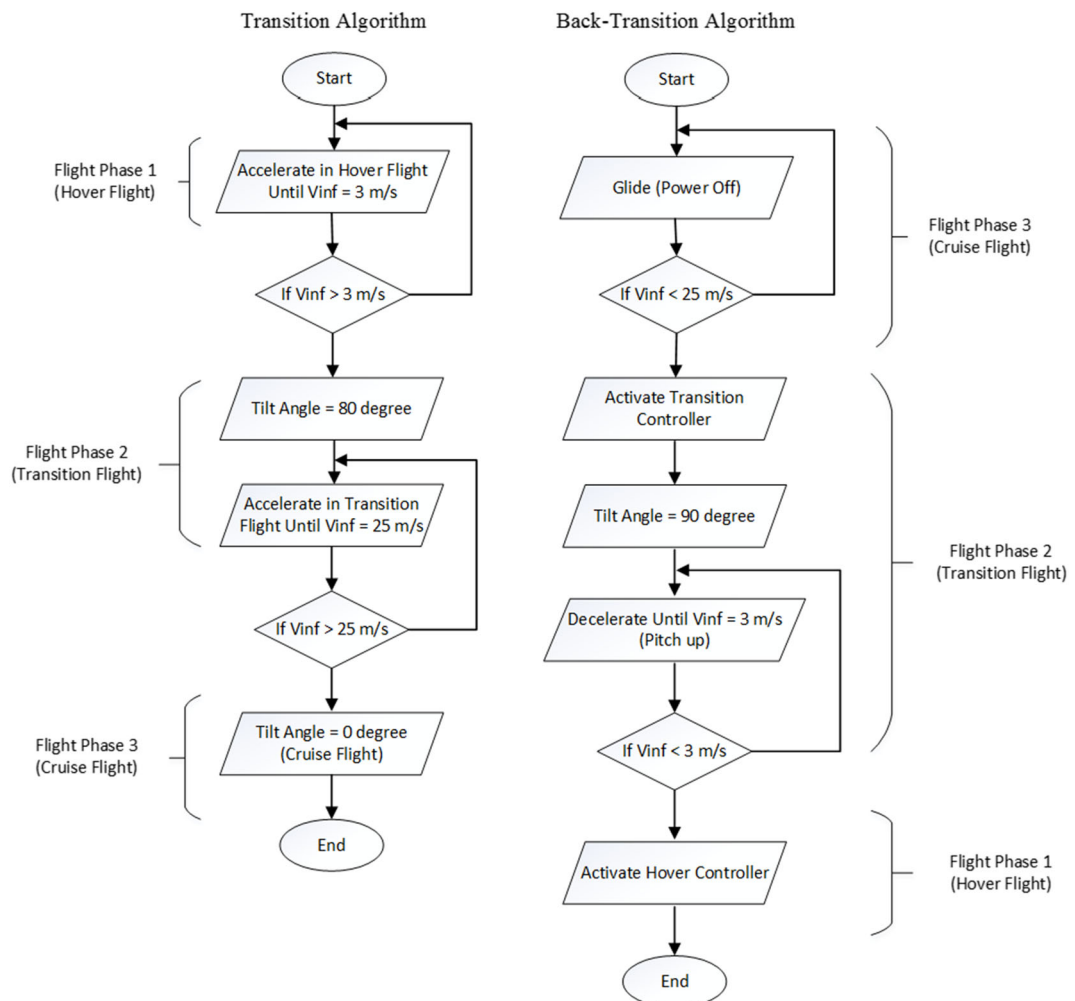


Fig. 22 Transition and back transition algorithms

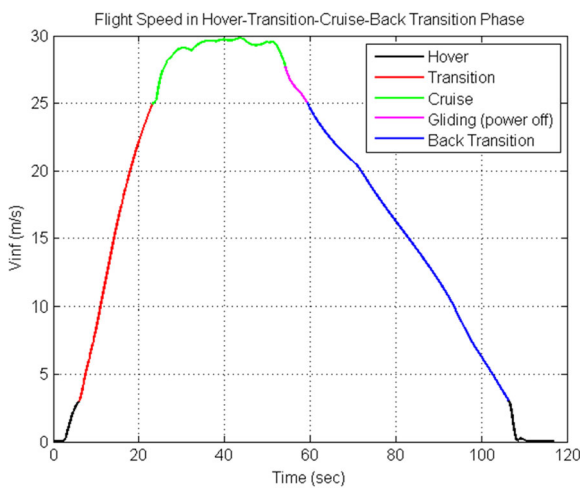


Fig. 23 The change of airspeed during the flight simulation

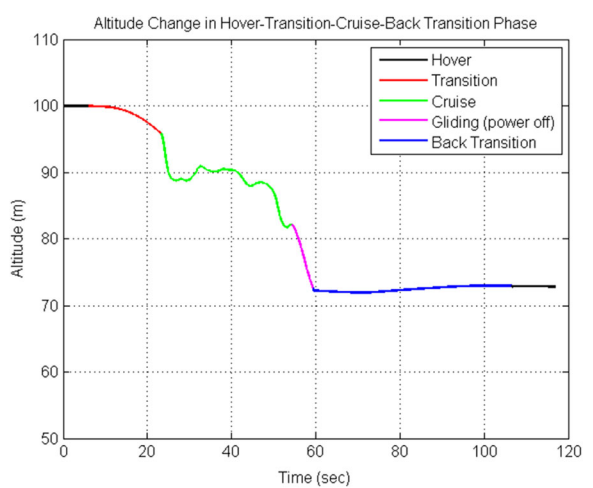


Fig. 24 The change of altitude during the flight simulation

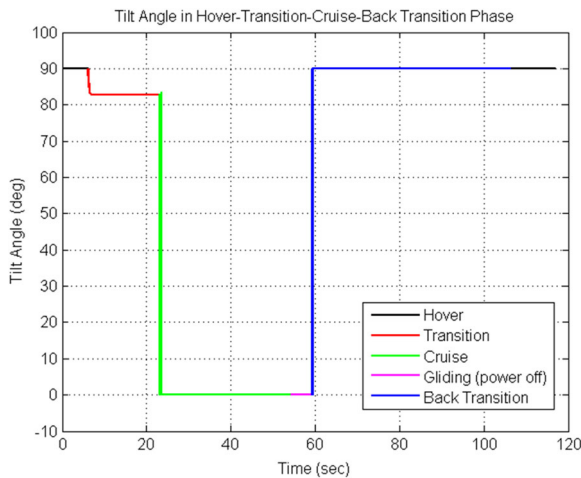


Fig. 25 The change of tilt angle during the flight simulation

flight (hover – transition – cruise - back transition – hover) of the TURAC is simulated for about 120 sec. The abovementioned algorithms are used in flight phase switching system.

Simulation results are shown in Figs. 23, 24, 25 and 26. Each flight regime is represented in different colors and labeled on the graphs.

In Fig. 23, hover flight is performed until the flight speed reaches to 3m/s (black region). Then transition flight regime starts, tilt-rotors are positioned at 90° and TURAC accelerates until 25m/s (red region). After that, horizontal flight controllers are activated and the UAV performs horizontal flight about $29 - 30\text{m/s}$ (green region). Before the back-

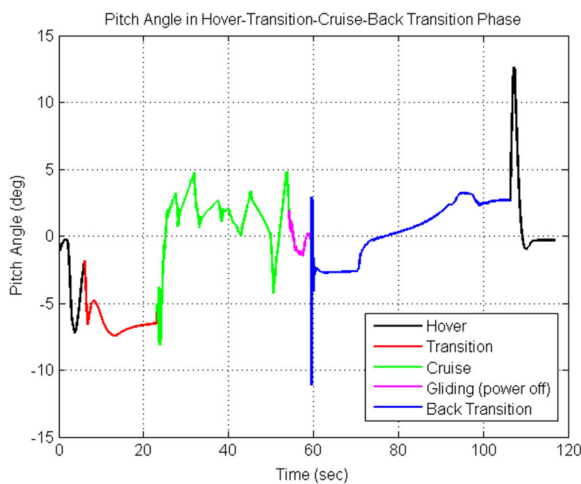


Fig. 26 The change of pitch angle during the flight simulation

transition regime, power of the tilt-rotor group is cut-off, the UAV starts to glide and flight speed decreases to 25m/s (magenta region). The back-transition flight regime starts when the flight speed goes down below 25m/s and continue until the hover flight speed limit, 3m/s (blue region). Finally, hover flight controllers are activated by the algorithm and flight speed



Fig. 27 Experimental transition maneuver demonstration

decreases to 0m/s in hover flight (black region at the end of the flight).

Altitude change is shown in Fig. 24. In hover flight, altitude remains constant for several seconds at 100m . Then, the transition flight starts and the altitude decreases about 5m because of the transition maneuver. After the transition regime, the horizontal flight starts and performed around 90m altitude. Before the back-transition, gliding flight is performed around $82 - 72\text{m}$ altitude and then transition controller is activated around 72m altitude. The tilt angle is set to 90° and the flight speed of the UAV is decreased at almost constant altitude with pitch-up motion. Finally, when the flight speed decreases below 3m/s , hover control system is activated by the algorithm and the UAV completes the back-transition maneuver.

Tilt angle of the front propellers is shown in Fig. 25. In hover flight, tilt-rotors are positioned at 90° . In transition, they are positioned at 82° and the UAV starts to accelerate. Then, the tilt angle is set to 0° and the UAV performs the cruise flight. After the gliding flight, tilt angle is set to 90° by the back-transition algorithm.

Pitch angle of the UAV during the flight is shown in Fig. 26. The pitch angle is used for accelerating and decelerating in hover and back-transition flight regimes. In hover flight, the flight speed of the UAV is increased by pitch-down motion (black range). At the end of the flight, in back-transition and hover flights, the speed of the UAV is decreased by giving a pitch-up command as shown in Fig. 26 between $70^\circ - 90^\circ$ seconds.

Using the described control system methodology, we have demonstrated the hover to transition maneuver with TURAC. Figure 27 shows the step by step forward flight transition of TURAC.

5 Conclusion

In this paper, we provide the complete six-degree-of-freedom nonlinear mathematical model of a tilt rotor unmanned aerial vehicle (UAV) including hover, forward flight and transition regimes. This model includes the aerodynamic effect of propeller-induced airstream, aerodynamic coefficients of the airframe and the airspeed dependent characteristics of the thrust-propellers.

Transition (hover to forward flight) and back-transition (forward flight to hover) scenarios are investigated and designed for the TURAC UAV. Transition scenarios as designed consist of a schedule for flight velocity, angle of attack, and thrust levels of both the tilt-rotors and coaxial fans and are used as a feedforward data set for the flight control system. Transition algorithms between hover-to-cruise and cruise-to-hover algorithms are described step-by-step. Real time 6-DoF simulations are performed for hover-to-cruise and cruise-to-hover flight by using the transition scenario datasets.

We present the simulation results of the transition control system and show the successful transition of TURAC in experiment.

Acknowledgments Research is supported in part by the Republic of Turkey, Ministry of Science, Industry and Technology and HAVELSAN Inc. (SANTEZ Program Contract No: 1585.STZ.2012-2).

References

1. Foy, B.W.: Hover Controls for a Unique Small-Scale Thrust Reversing UAV, MSc. University of Colorado, Thesis (2005)
2. Ozdemir, U., Aktas, Y.O., Vuruskan, A., Dereli, Y., Tarhan, A.F., Demirbağ, K., Erdem, A., Kalaycioglu, G.D., Ozkol, I., Inalhan, G.: Design of a commercial hybrid VTOL UAV system. *J. Intell. Robot. Syst.* **74**, 371–393 (2014)
3. Aktas, Y.O., Ozdemir, U., Dereli, Y., Tarhan, A.F., Cetin, A., Vuruskan, A., Yuksek, B., Cengiz, H., Basdemir, S., Ucar, M., Genctav, M., Yukseken, A., Ozkol, I., Kaya, M.O., Inalhan, G.: A low cost prototyping, analyzing and flight testing for the TURAC VTOL UAV, ICUAS 2014, Orlando, May 27-30 (2014)
4. Aktas, Y.O., Ozdemir, U., Dereli, Y., Tarhan, A.F., Cetin, A., Vuruskan, A., Yuksek, B., Cengiz, H., Basdemir, S., Ucar, M., Genctav, M., Yukseken, A., Ozkol, I., Kaya, M.O., Inalhan, G.: A low cost prototyping, analyzing and flight testing for the TURAC VTOL UAV, Submitted for Review for Publication ICUAS 2014, Orlando, May 27-30 (2014)
5. Gupta, V.: Quad tilt rotor simulations in helicopter mode using computational fluid dynamics. University of Maryland, PhD thesis (2005)
6. Postdam, M.A., Strawn, R.C.: CFD simulations of tiltrotor configurations in hover, at the American Helicopter Society 58th Annual Forum June, 11–13 (2002)
7. Young, L.A., Lillie, D., McCluer, M., Yamauchi, G.K.: Insights into airframe aerodynamics and rotor-on-wing interactions from a 0.25-scale tiltrotor wind tunnel model,

- A.S International Aerodynamics, Acoustics, and Test and Evaluation Specialists' Conference, San Francisco, CA, January 23–25 (2002)
- 8. Yeo, H., Johnson, W.: Performance and design investigation of heavy lift tilt-rotor with aerodynamic interference effects. *J. Aircr.* **46**(4), 1231–1239 (2009)
 - 9. Cummings, R.M., Morton, S.A., Siegel, S.G.: Numerical prediction and wind tunnel experiment for a pitching unmanned combat air vehicle. *Aerosp. Sci. Technol.* **12**, 355–364 (2008)
 - 10. Wisnöe, W., Nasir, R.E.M., Kuntjoro, W., Mohd, A., Mamat, I.: Wind tunnel experiments and CFD analysis of Blended Wing Body (BWB) Unmanned Aerial Vehicle (UAV) at mach 0.1 and mach 0.3. In: 13th International conference on Aerospace Sciences & Aviation Technology, ASAT-13, May 26–28 (2009)
 - 11. Lino, M.: Numerical investigation of propeller-wing interaction effects for a large military transport aircraft **27** (2010)
 - 12. Kim, C., Chung, J.: Aerodynamic analysis of tilt-rotor unmanned aerial vehicle with computational fluid dynamics. *J. Mech. Sci. Technol.* **20**(4), 561–568 (2006)
 - 13. Abbas, J., Narducci, R.: Analysis of CFD modeling techniques over the mv-22 tiltrotor. In: American Helicopter Society 66th Annual Forum, Phoenix, AZ, May 11–13 (2010)
 - 14. Sweeten, B.: CFD analysis of UAVs using Vorstab, Fluent, and Advanced Aircraft Analysis software **27** (2010)
 - 15. Tekinalp, O., Unlu, T., Yavrucuk, I.: Simulation and flight control of a tilt duct UAV, Tekinalp, Unlu, Yavrucuk, AIAA Modelling and Simulation Tech. Conf., Chicago, USA, 10–13 August 2009
 - 16. Flores, G.R., Escareno, J., Lozano, R., Salazar, S.: Quad-tilting rotor convertible MAV: Modelling and real-time hover flight control. *J. Intell. Robot. Syst.* **65**, 457–471 (2012)
 - 17. Flores, G., Lozano, R.: Transition flight control of the quad-tilting rotor convertible MAV. In: 2013 International Conference on Unmanned Aircraft Systems (ICUAS), Atlanta, May 28–31 (2013)
 - 18. Matos, C., Reddy, U., Komerath, N.: Rotor wake/fixed wing interactions with flap deflection, American Helicopter Society 55th Annual Forum, Montreal, Canada, May, 25–27 (1999)
 - 19. Matos, C.A.M.: Download reduction on a wing-rotor configuration. Georgia Institute of Technology, PhD thesis (December 2001)
 - 20. Nelson, R.C.: Flight Stability and Automatic Control, 2nd ed., Singapore, McGraw-Hill, ch.3–5 (1998)
 - 21. Blakelock, J.H.: Automatic Control of Aircraft and Missiles, 2nd ed., USA: John Wiley & Sons, ch. 1,3 (1991)
 - 22. Yechout, T.R.: Introduction to Aircraft Flight Mechanics, VA: AIAA Education Series, ch. 4–6 (2003)
 - 23. Advisory Group for Aerospace Research and Development (AGARD): The Aerodynamics of V/STOL Aircraft, AGARDograph 126 (1968)

B. Yuksek is a PhD students at Istanbul Technical University.

A. Vuruskan is a PhD students at Istanbul Technical University.

U. Ozdemir is a PhD candidate at Istanbul Technical University.

M. A. Yukselen is a Professor at Istanbul Technical University.

G. Inalhan is a Associate Professor at Istanbul Technical University.